

ORIGINAL ARTICLE

Role of Aluminium on the Microstructure and Corrosion Behaviour of Magnesium Prepared by Powder Metallurgy Method

J. Alias*

Structural Material and Degradation (SMD) Focus Group, Faculty of Mechanical Engineering, Universiti Malaysia Pahang, 26600 Pekan, Pahang
Phone: +6094246227; Fax: +6094246222

ABSTRACT – Much research on magnesium (Mg) emphasises creating good corrosion resistance of magnesium, due to its high reactivity in most environments. In this study, powder metallurgy (PM) technique is used to produce Mg samples with a variation of aluminium (Al) composition. The effect of aluminium composition on the microstructure development, including the phase analysis was characterised by optical microscope (OM), scanning electron microscopy (SEM) and x-ray diffraction (XRD). The mechanical property of Mg sample was performed through Vickers microhardness. The results showed that the addition of aluminium in the synthesised Mg sample formed distribution of Al-rich phases of $Mg_{17}Al_{12}$, with 50 wt.% of aluminium content in the Mg sample exhibited larger fraction and distribution of Al-rich phases as compared to the 20 wt.% and 10 wt.% of aluminium content. The microhardness values were also increased at 20 wt.% and 50 wt.% of aluminium content, comparable to the standard microhardness value of the annealed Mg. A similar trend in corrosion resistance of the Mg immersed in 3.5 wt.% NaCl solution was observed. The corrosion behaviour was evaluated based on potentiodynamic polarisation behaviour. The corrosion current density, i_{corr} , is observed to decrease with the increase of Al composition in the Mg sample, corresponding to the increase in corrosion resistance due to the formation of aluminium oxide layer on the Al-rich surface that acted as the corrosion barrier. Overall, the inclusion of aluminium in this study demonstrates the promising development of high corrosion resistant Mg alloys.

ARTICLE HISTORYRevised: 15th Sept 2020Accepted: 22nd Sept 2020**KEYWORDS***Aluminium; Magnesium; Microstructure, Corrosion; Powder metallurgy*

INTRODUCTION

Magnesium (Mg) and its alloys are known to have good strength, low density and good machinability. Mg is comparable to steel and aluminium as the promising metals used in many industries due to its lightweight properties and capability to reduce CO₂ consumption [1, 2]. In medical purposes, Mg has aroused attention for its biocompatibility and biodegradable characters. Mg features mechanical properties that are closer to the bone, and it is absorbable by the human body. The unharmed of Mg content in the human body can be used to produce new bone material, and excess of Mg levels are easily processed by the kidney and released in the urine [3–6]. The use of Mg as a temporary implant due to its high degradation rate is gaining significant interest.

Mg offers biocompatibility and significantly reduced the stress shielding problems of implants, making Mg a suitable candidate for temporary body implants [7, 8]. However, Mg's major drawbacks come from the high degradation rate in the body and poor corrosion resistance in most environments. Much research has been taken to focus on modifying the microstructure by alloying, heat treatments, and applying common corrosion protection methods such as coatings and inhibitors as the alternative method to improve its corrosion resistance [9–14].

Consideration of the microstructure is essential to create material with improvement to both strength and corrosion resistance [15–17]. Grain structure and phases formation effects are usually correlated to the increase in strength, which compromise the corrosion [3, 18–20]. Aluminium has been added in commercial Mg alloy, to improve their strength by solid solution hardening [21, 22]. The addition of aluminium leading to the precipitation of β - $Mg_{17}Al_{12}$ phases that usually occurs at the grain boundaries [23–25]. Park et al. [26] mentioned variation of precipitates form from the addition of Mg to Al sample, including Al_3Mg_2 , $Mg_{17}Al_{12}$, and the oxides particles affected the Vickers hardness. Miao et al. [25] suggested that the alloying addition to Mg-Al material significantly changed the morphology of $Mg_{17}Al_{12}$ phases and, consequently, enhanced the ageing response and strength.

Mg alloys were produced with a variation of aluminium composition using the powder metallurgy (PM) method. The promising properties of metals by PM method is including the reduction of porosity, grain refinement, economical and less time consuming [3, 15, 27]. This present work deals with the investigation of the effect of aluminium variation on the microstructure evolution and corrosion behaviour of the Mg alloy prepared by PM method.

EXPERIMENTAL PROCEDURE

In this study, Mg (99.5 wt.% purity) and aluminium powders (99.2 wt.% purity) were used to synthesise Mg-Al alloys, purchased from Vistec Technology Sdn Bhd. The Mg powder is in a spherical shape with a size of 40-60 microns and 6-10 microns size of aluminium powder. Mg with three variations of aluminium composition was prepared by weighing using an analytical balance. The compositions of produced samples include Mg-10 wt.% Al, Mg-20 wt.% Al and Mg-50 wt.% Al.

The mixture of the powders was mechanically alloyed by blended and milled with planetary ball mill, PM100 for 2 hours, using 30 stainless steel balls at 200 rpm of milling speed. The ball-powder ratio (BPR) is set to 20:1 to each of the ball milling processes. Figure 1 shows the scanning electron microscopy (SEM) image of the sample powder after the ball milling process. The powders were then uniaxially pressed into a green compact (an unsintered compact) at the pressure of 300 MPa to a disc-shaped with a diameter of 25 mm. The green compact sample was further sintered to a brown compact (a sintered compact) at the temperature of 500°C for 1 hour. Sintering was carried out in the tube furnace under a nitrogen gas atmosphere to avoid the formation of oxide and burn of the sample. Figure 2 presents the fabrication route for the synthesis of Mg-Al alloys.

Samples for microstructure were sectioned, mounted and mechanically ground to 2500 grit paper, and further polished with 3, 1-micron diamond and alumina colloidal suspension. The sample was then etched using glycol etchant. The microstructure observation was performed under an optical microscope (Olympus) and a scanning electron microscopy (SEM) (FEI Quanta 450), equipped with energy-dispersive x-ray spectroscopy (EDS). The phase composition of the samples was identified by X-ray diffraction (XRD, PANalytical X'pert³ powder). The pattern was recorded from 10 to 90° 2 theta using cobalt K α radiation for phase identification. The similar sample was applied for Vickers microhardness for 3 indentations for accuracy and reproducibility. The Vickers hardness test was conducted with 100 gf load and dwell time of 10 s. Electrochemical measurement was then performed by the potentiodynamic polarisation method. Three-electrode electrochemical cell is used consisting of the sample as a working electrode, graphite as the counter electrode and saturated calomel electrode (SCE) as the reference electrode, and immersed in 3.5 wt.% NaCl solution as the electrolyte. The scan rate was 1 mV/s, with applied initial potential of -2 V to the final potential of 0.2 V. All potentials are reported with respect to a saturated calomel electrode (SCE). All tests and solutions were quiescent and naturally aerated at 25°C.

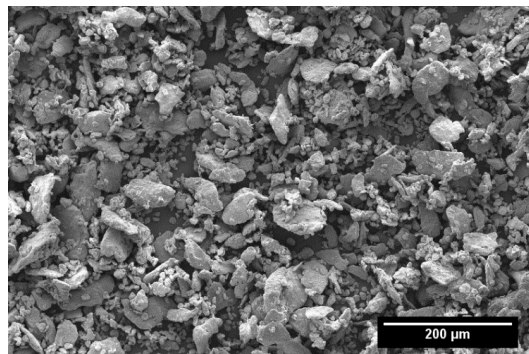


Figure 1. SEM image of Mg powder after ball milled.

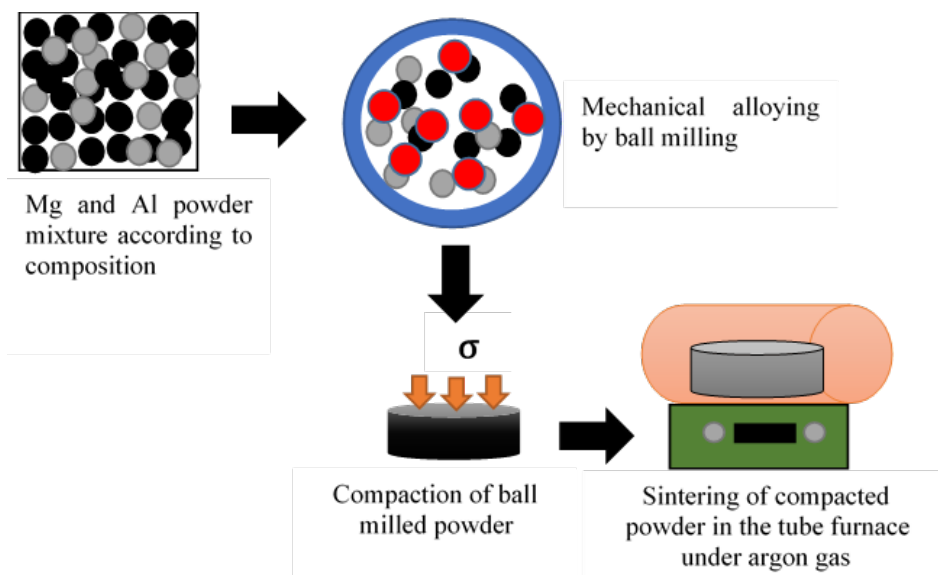


Figure 2. Fabrication route for synthesis Mg-Al alloys.

RESULT AND DISCUSSION

Morphology and Microstructure Observation

Figures 3(a) to 3(c) show the optical images of Mg samples with different aluminium composition; sintered at 500 °C for 1-hour duration. The sample displayed a different appearance in which the Mg-10 wt.% Al sample in Figure 3 (a) having a brownish-like colour, which is darker than Mg-20 wt.% Al sample in Figure 3 (b). Figure 3(c) displays Mg-50 wt.% Al sample showing a much darker sample than the other samples. The different appearance of each sample depends on the sintering condition and the alloying composition. The mixture of powder produced a good brown compact sample after the sintering, although some of the sample edges indicated brittleness.

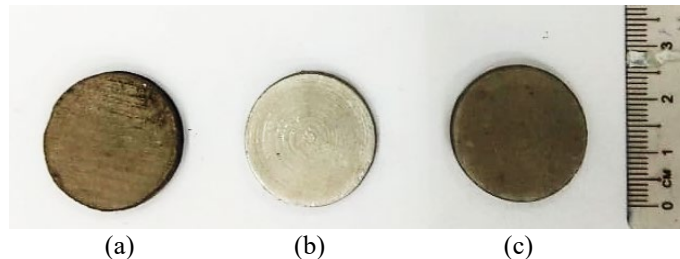
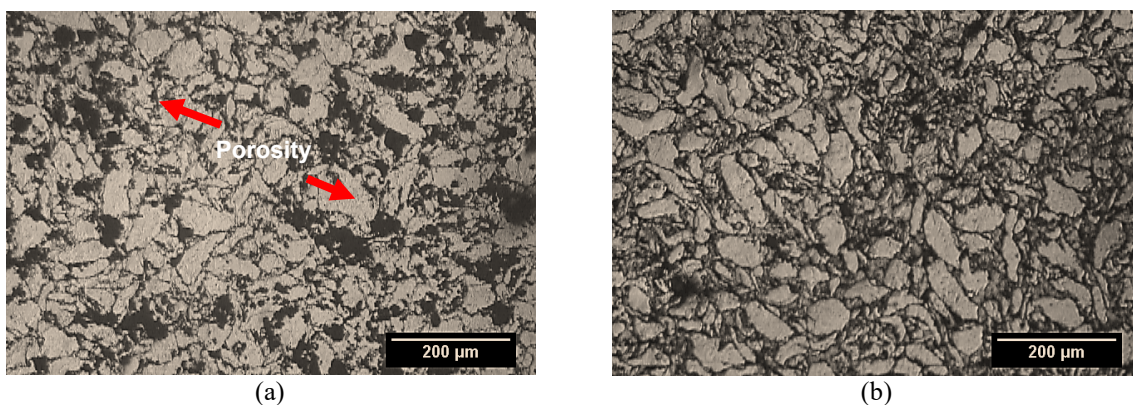


Figure 3. Images of sintered Mg sample (a) Mg-10 wt.% Al; (b) Mg-20 wt.% Al; and (c) Mg-50 wt.% Al.

The material consists of the distribution of second phase particles of the Al-rich and Mg matrix from the microstructure observation. Figure 4(a) to 4(c) display the micrographs of the samples taken at bright field mode of optical microscopy. The composition of Mg-10 wt.% Al is shown in Figure 4(a) clearly indicating porosities in the sample, which are displayed as the dark features in the sample. The average size of pores is about 48 μm , as measured by the ImageJ software. The porosities are expected to be located at the area adjacent to the Al-rich phases, as evident in Figures 4(b) and 4(c). The increase of another 10 wt.% of aluminium content in the Mg sample reduced the porosities distribution and size and revealed the Al-rich phases in the Mg-20 wt.% Al sample.

According to Mg-Al binary phase diagram [28], during sintering temperature (500 °C), which is above 437 °C, the Al reacts with pure Mg to form Mg-Al liquid phase. The Mg-Al liquid phase was then precipitated as solid Mg and $\text{Mg}_{17}\text{Al}_{12}$ intermetallic phase upon cooling. The distribution of Al-rich phases which is regarded as $\text{Mg}_{17}\text{Al}_{12}$ phases, can be seen slightly darker than the matrix forming a boundary to the matrix region (Figure 4(b)). Figure 4(c) shows the composition of Mg-50 wt.% Al sample, which exhibited a large fraction and distribution of $\text{Mg}_{17}\text{Al}_{12}$ phases, with an average particle diameter of 85 μm , measured by the ImageJ software. The phases are evidenced in much darker features and lamellar type structure, as magnified in the inset figure. The morphology of eutectic or intermetallic phases of $\text{Mg}_{17}\text{Al}_{12}$ gradually evolved from a random distribution to network or continuous phases with the increase of Al addition [29].

Porosities exist in the sample, with a reduction in size compared to the porosities in Mg-10 and 20 wt.% Al sample. It is found that porosity could be reduced by increasing the compaction pressure, sintering temperature and sintering time [30,31]. The inclusion of a high amount of alloying is commonly contributed to the porosity; however formation of the porosity can also be influenced by the types of alloying element in the metal [32,33].



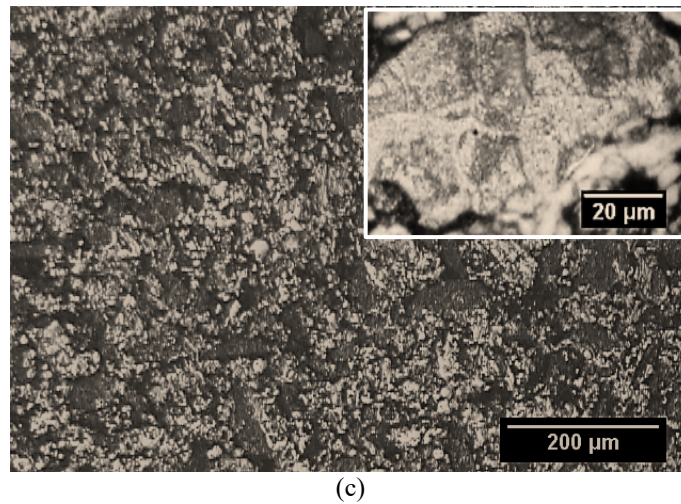
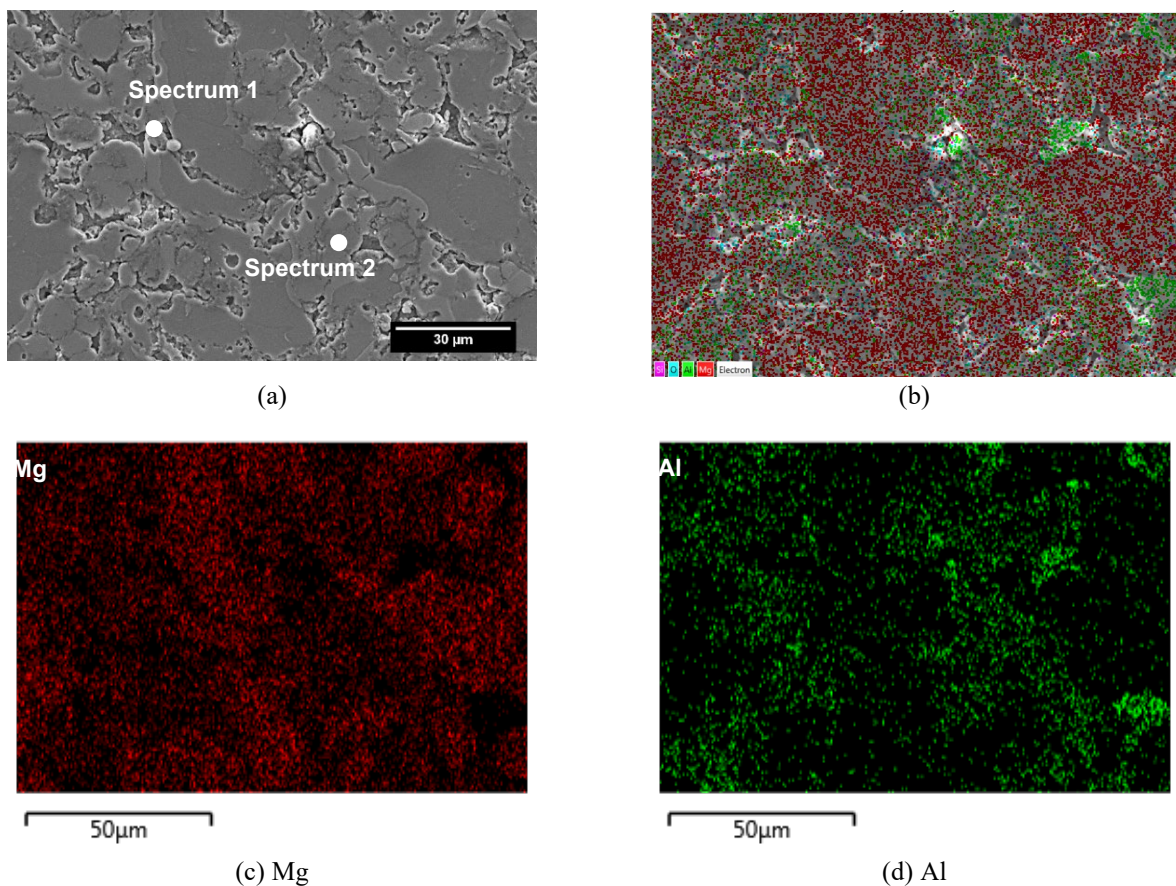


Figure 4. Optical micrographs of (a) Mg-10 wt.% Al; (b) Mg-20 wt.% Al; and (c) Mg-50 wt.% Al with magnified image.

Figure 5 shows the SEM image, EDS composition map and spectrum of Mg-20 wt.% Al. The localise composition mapping proved the existence of the Mg matrix as depicted in Spectrum 1, with 91.3 wt.% Mg and balance of Al. The $Mg_{17}Al_{12}$, Al-rich phases, indicated 93.27 wt.% of Al and balance of Mg, displayed in spectrum 2. The peak of oxygen or oxide was also present in the spectrum; however, it is disregarded in the analysis due to undesirable inclusion/contamination. It is also believed that the inclusion of oxide can be sourced from the porosity [34]. From the SEM image, most of the porosities can be seen located adjacent to the $Mg_{17}Al_{12}$ phases. The $Mg_{17}Al_{12}$ phases distributed in a network, and the porosities were forming boundaries to the Mg-matrix. The XRD analysis indicated that the existence of $Mg_{17}Al_{12}$ phases as the Al-rich phases is matched and confirmed in the sample, as depicted in Figure 6. Higher peak intensity of the $Mg_{17}Al_{12}$ was observed at 35° 2 theta angle, indexed at the basal plane (0002). No peaks of other phases were detected, as established in the phase diagram of Mg-Al. According to [24,35] the intermetallic particles of $Mg_{17}Al_{12}$ are commonly formed parallel to the basal plane (0001), where the dislocation slips in the Mg matrix mostly occur. Thus, the high amount of these particles can improve the mechanical properties of Mg alloys.



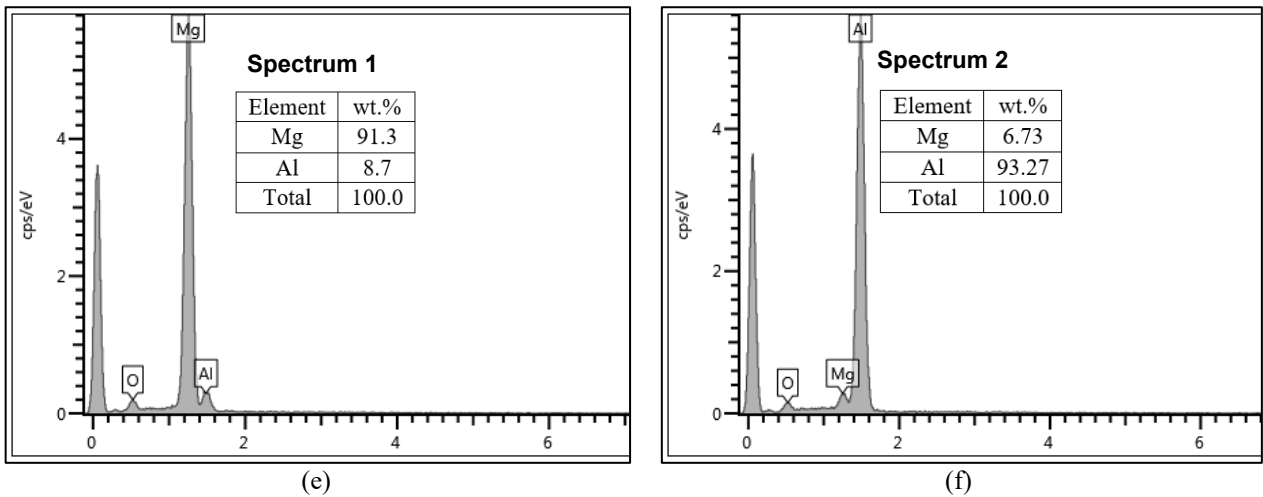


Figure 5. (a), (b) SEM image and EDS composition mapping (c), (d) and spectrum (e), (f) of Mg-10 wt.% Al sample.

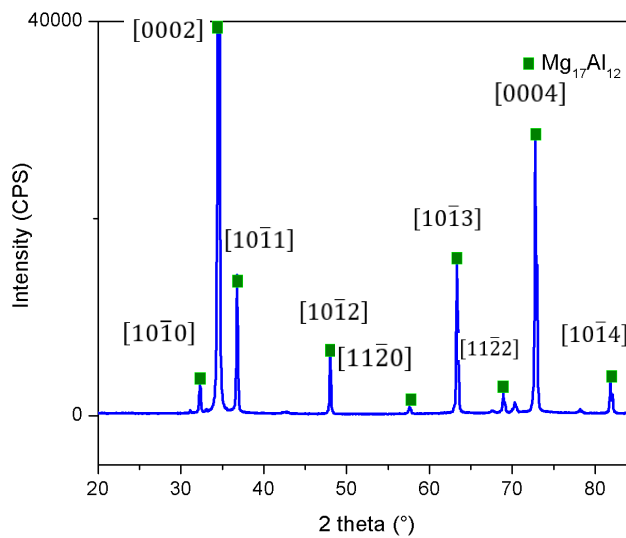


Figure 6. XRD analysis indicating $Mg_{17}Al_{12}$ as the phases of the Al-rich region.

Hardness Measurement

Vickers microhardness was conducted to the Mg samples. The hardness value is influenced by the chemical composition and microstructure development during sintering. Three (3) hardness measurements were conducted on the sample. The average hardness value is shown in Table 1, indicating the increase of hardness value with more amount of aluminium content. A higher fraction of aluminium rich region shows the increase of hardness value. The high Al content induces the formation of main intermetallic phase ($Mg_{17}Al_{12}$) in the Mg-Al alloys, which is a hard and brittle phase with the microhardness about 280 HV [24,36]. Thus, improved the hardness of the overall Mg sample. The average microhardness values of Mg-20 wt.% Al and Mg-50 wt.% Al are HV80.07 and HV86.7, respectively, which are slightly higher than the standard microhardness value of the Mg sample (HV74) [37].

Table 1. Average Vickers microhardness.

Sample	Hardness (HV)			Average
	Indentation point			
	1	2	3	
Mg-10 wt.%Al	69.8	71.2	70.4	70.47
Mg-20 wt.%Al	80.5	80.4	79.3	80.07
Mg-50 wt.%Al	88.7	84.7	86.7	86.70

Polarisation Behaviour

Figure 7 shows the potentiodynamic polarisation curve of the Mg samples immersed in 3.5 wt.% NaCl solution. The corrosion current density, i_{corr} decreases with the increase of Al composition, and no passivation can be seen from the curve. The addition of 20 wt.% Al yields similar trend of results to the addition of 50 wt.% of Al; with the i_{corr} decreases from 0.0001659 to 0.0000794 A/cm². Less i_{corr} value determines the increase in corrosion resistance. During immersion, Mg dissolution was observed at the matrix, with continuous hydrogen gas evolved. Microgalvanic corrosion occurred

attributed by the presence of $Mg_{17}Al_{12}$ that served as the cathode, while the Mg matrix as the anode. It is obvious that most of the $Mg_{17}Al_{12}$ phases did not dissolve and stable during the corrosion. The increase of corrosion resistance of Mg is attributed to the presence of large fraction or distribution of the Al-rich phases or $Mg_{17}Al_{12}$, that acts as a corrosion barrier [38,39]. Variation aluminium distributions could promote different corrosion mechanisms and Al-rich or β -phase, $Mg_{17}Al_{12}$ acts as an efficient cathode with a strong galvanic couple at the β -phase/surrounding material interface [40]. Large fraction and distribution of the phase induced aluminium oxide (Al_2O_3) layer on the particle surface that prevents corrosion progression. Al_2O_3 known to be less soluble and stable than MgO and $Mg(OH)_2$ in neutral solution. The enrichment of alumina would affect the anodic reaction by acting to reduce the current density and thus, improve corrosion properties [41]. A schematic illustration of the corrosion mechanism of Mg with $Mg_{17}Al_{12}$ phases is displayed in Figure 8.

The high amount of porosities presents in 10 wt.% Al compared to 50 wt.% Al content is expected to be the corrosion initiation point, contributing to the high corrosion current density, i_{corr} . Aghion and Perez [42] pointed out that the corrosion resistance of Mg alloy is significantly affected by the porosity content, in which, high amount of porosity increases the corrosion rate of Mg alloy calculated by Tafel extrapolation. Porosity increases the passive current density and lowers the stability of the passive film [43]. A small shift in the cathodic curve of Mg-20 wt.% Al than the Mg-10 wt.% Al is revealed, while a larger shift of cathodic curve is obtained to Mg-50 wt.% Al, approximately higher +0.2 V of corrosion potential to about -1.38 V, with reference to SCE. Table 2 lists out the polarisation result obtained from the polarisation curve.

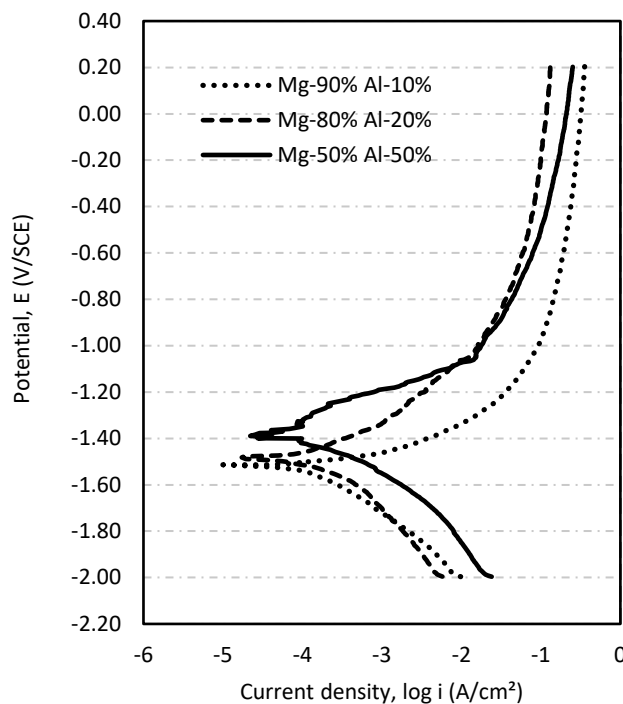


Figure 7. Potentiodynamic polarisation curve of Mg-Al samples with variation composition, immersed in 3.5 wt.% NaCl solution.

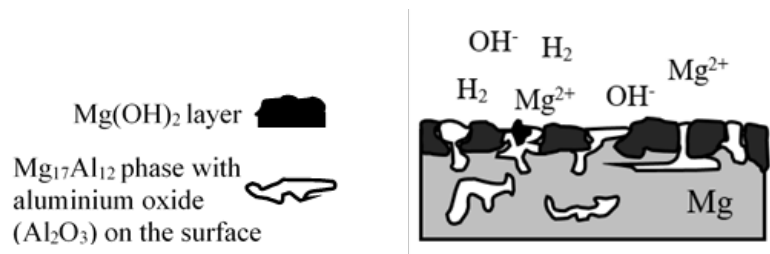


Figure 8. A schematic illustration of Mg with $Mg_{17}Al_{12}$ phases during the corrosion process.

Table 2. E_{corr} and i_{corr} value during potentiodynamic polarisation of samples in 3.5 wt.% NaCl solution.

Sample	E_{corr} (V/SCE)	i_{corr} (A/cm ²)
Mg-10 wt.% Al	-1.555	0.001259
Mg-20 wt.% Al	-1.441	0.0003162
Mg-50 wt.% Al	-1.306	0.0001585

CONCLUSION

The effect of aluminium variation on the microstructure development was observed. α -Mg matrix and Al-rich phases of $Mg_{17}Al_{12}$ were formed in the sample with the presence of porosities, especially with less aluminium. The addition of 50 wt.% of Al introduced a large fraction of $Mg_{17}Al_{12}$ phases of the Mg-Al sample compared to 20 and 10 wt.% Al of Mg sample. Aluminium addition also significantly increased the microhardness of sample (HV86.7 for Mg-50 wt.% Al), higher than the standard microhardness value of Mg sample (HV74, annealed Mg). Based on the polarisation behaviour, the increment of 50 wt.% of aluminium shifted the cathodic branch to more electropositive (corrosion potential of -1.38 V). The corrosion current density, i_{corr} decreases with the increase of Al composition, corresponding to the increase in corrosion resistance. A large fraction of $Mg_{17}Al_{12}$ phase induced aluminium oxide layer on the surface of the phase that prevents corrosion progression and acts as a corrosion barrier. Thus, the higher fraction of aluminium does increase the resistant to further corrosion.

ACKNOWLEDGEMENT

The authors are grateful to Universiti Malaysia Pahang (Research grant RDU180333) for financial support.

REFERENCES

- [1] Luo AA. Magnesium development as a lightweight material-In competition with other structural materials. In: Solanki KN, Orlov D, Singh A, et al. (eds) Magnesium Technology 2017. Cham: Springer International Publishing, 2017, p. 7.
- [2] Kulkarni S, Edwards DJ, Parn EA, et al. Evaluation of vehicle lightweighting to reduce greenhouse gas emissions with focus on magnesium substitution. *Journal of Engineering, Design and Technology* 2018; 16: 869–888.
- [3] Ali M, Hussein MA, Al-Aqeeli N. Magnesium-based composites and alloys for medical applications: A review of mechanical and corrosion properties. *Journal of Alloys and Compounds* 2019; 792: 1162–1190.
- [4] Farraro KF, Kim KE, Woo SLY, et al. Revolutionising orthopaedic biomaterials: The potential of biodegradable and bioresorbable magnesium-based materials for functional tissue engineering. *Journal of Biomechanics* 2014; 47: 1979–1986.
- [5] Zhang S, Zhang X, Zhao C, et al. Research on Mg-Zn alloy as a degradable biomaterial. *Acta biomaterialia* 2010; 6: 626–40.
- [6] Wang C, Yi Z, Sheng Y, et al. Development of a novel biodegradable and anti-bacterial polyurethane coating for biomedical magnesium rods. *Materials Science and Engineering: C* 2019; 99: 344–356.
- [7] Ali M, Hussein MA, Al-Aqeeli N. Magnesium-based composites and alloys for medical applications: A review of mechanical and corrosion properties. *Journal of Alloys and Compounds* 2019; 792: 1162–1190.
- [8] Hänni AC, Gerber I, Schinhammer M, et al. On the in vitro and in vivo degradation performance and biological response of new biodegradable Mg-Y-Zn alloys. *Acta biomaterialia* 2010; 6: 1824–33.
- [9] Matsuda T, Kashi KB, Fushimi K, et al. Corrosion protection of epoxy coating with pH sensitive microcapsules encapsulating cerium nitrate. *Corrosion Science* 2018; 148: 188–197.
- [10] Manne B, Bontha S, Ramesh MR, et al. Solid state amorphisation of Mg-Zn-Ca system via mechanical alloying and characterisation. *Advanced Powder Technology* 2017; 28: 223–229.
- [11] Pegguleryuz MO, Kainer KU, Arslan Kaya A, et al. Alloying behavior of Magnesium and alloy design. In: *Fundamentals of Magnesium Alloy Metallurgy*. Woodhead Publishing Limited, 2013, pp. 152–196.
- [12] Yan Y, Cao H, Kang Y, et al. Effects of Zn concentration and heat treatment on the microstructure, mechanical properties and corrosion behavior of as-extruded Mg-Zn alloys produced by powder metallurgy. *Journal of Alloys and Compounds* 2017; 693: 1277–1289.
- [13] Tamang S, Potaliya P, Aravindan S. Corrosion behaviour of magnesium–yttria composite sintered by microwave hybrid heating. *Materials Research Innovations* 2017; 8917: 1–5.
- [14] Chandrasekaran M, John YMS. Effect of materials and temperature on the forward extrusion of magnesium alloys. *Materials Science and Engineering: A* 2004; 381: 308–319.
- [15] Medina J, Pérez P, Garcés G, et al. A High-strength Mg-6Zn-1Y-1Ca (wt %) alloy containing quasicrystalline I-phase processed by a powder metallurgy route. *Materials Science & Engineering A* 2018; 715: 92–100.
- [16] Kawamura Y, Hayashi K, Inoue A, et al. Rapidly solidified powder metallurgy magnesium alloys with novel mechanical properties. In: *Proceedings of the International Symposium on Metastable, Mechanically Alloyed and Noncrystalline Materials (ISMANAM)*, pp. 529–534; 2002.
- [17] Dvorsky D, Kubasek J, Vojtěch D, et al. Preparation of WE43 using powder metallurgy route. *Manufacturing Technology* 2016; 16: 680–687.
- [18] Alias J, Harun WSW, Ayu HM. A review on the preparation of magnesium-based alloys prepared by powder metallurgy and the evolution of microstructure and mechanical properties. *Key Engineering Materials* 2019; 796: 3–10.
- [19] Mohamed NS, Alias J. The influence of friction stir welding of dissimilar az31 and az91 magnesium alloys on the microstructure and tensile properties. *International Journal of Automotive and Mechanical Engineering* 2019; 16: 6675-6683.
- [20] Alias J, Zhou X, Das S, et al. Microstructure evolution and texture development of hot form-quench (HFQ) AZ31 twin roll cast (TRC) magnesium alloy. *AIP Conference Proceedings* 2017; 1901(1):130005.
- [21] Nie J-F. Precipitation and Hardening in Magnesium Alloys. *Metallurgical and Materials Transactions A* 2012; 43: 3891–3939.

- [22] Stulikova I, Smola B, Vlach M, et al. Influence of powder metallurgy route on precipitation processes in MgTbNd alloy. *Materials Characterization* 2016; 112: 149–154.
- [23] Ren YP, Qin GW, Pei WL, et al. The α -Mg solvus and isothermal section of Mg-rich corner in the Mg-Zn-Al ternary system at 320 °C. *Journal of Alloys and Compounds* 2009; 481: 176–181.
- [24] Li Y, Tan C, Yu X, et al. Evolution of β Mg₁₇Al₁₂ in MgAlZnAg alloy over time. *Materials Science and Engineering: A* 2019; 754: 470–478.
- [25] Miao J, Sun W, Klamer AD, et al. Interphase boundary segregation of silver and enhanced precipitation of Mg₁₇Al₁₂ Phase in a Mg-Al-Sn-Ag alloy. *Scripta Materialia* 2018; 154: 192–196.
- [26] Park K, Park J, Kwon H. Effect of intermetallic compound on the Al-Mg composite materials fabricated by mechanical ball milling and spark plasma sintering. *Journal of Alloys and Compounds* 2018; 739: 311–318.
- [27] Fang ZZ, Paramore JD, Sun P, et al. Powder metallurgy of titanium – past, present, and future. *International Materials Reviews* 2017; 0: 1–53.
- [28] Okamoto H, Schlesinger ME, Mueller EM. *ASM Volume 3. Alloy Phase Diagrams*. Ohio: ASM International; 2004.
- [29] Zhang Y, Li M, Yang W-L, et al. Microstructural evolution and mechanical properties of as-cast Mg-12Zn alloys with different Al additions. *Materials Research* 2020; 23: 1-9.
- [30] Jabur AS. Effect of powder metallurgy conditions on the properties of porous bronze. *Powder Technology* 2013; 237: 477-483.
- [31] Durai TJ, Sivapragash M, Edwin Sahayaraj M. Effect of sintering temperature on mechanical properties of Mg-Zr alloy. *International Journal of Mechanical and Production Engineering Research and Development* 2017; 7: 117–122.
- [32] Candan E. Effect of alloying additions on the porosity of SiCp preforms infiltrated by aluminium. *Materials Letters* 2006; 60(9-10): 1204-1208.
- [33] Candan E, Atkinson HV, Jones H. Effect of alloying additions on threshold pressure for infiltration and porosity of aluminium-based melt infiltrated silicon carbide powder compacts. *Key Engineering Materials* 1997; 127-131: 463-470.
- [34] Čapek J, Vojtěch D. Effect of sintering conditions on the microstructural and mechanical characteristics of porous magnesium materials prepared by powder metallurgy. *Materials Science and Engineering C* 2014; 35: 21–28.
- [35] Ohno M, Mirkovic D, Schmid-Fetzer R. Phase equilibria and solidification of Mg-rich Mg–Al–Zn alloys. *Materials Science and Engineering: A* 2006; 421: 328–337.
- [36] Zhang L, Cao ZY, Liu YB, et al. Effect of Al content on the microstructures and mechanical properties of Mg–Al alloys. *Materials Science and Engineering: A* 2009; 508: 129–133.
- [37] Gopienko VG. Production of magnesium and magnesium alloy powders. In: Neikov OD, Naboychenko SS, Murashova IV, Gopienko VG, Frishberg IV, Lotsko DV, editors. *Handbook of Non-Ferrous Metal Powders*, Elsevier Science: Amsterdam, 2009, p 324–330.
- [38] Bu H, Yandouzi M, Lu C, et al. Cold spray blended Al+Mg₁₇Al₁₂ coating for corrosion protection of AZ91D magnesium alloy. *Surface and Coatings Technology* 2012; 207: 155–162.
- [39] Zhang X, Zhong F, Li X, et al. The effect of hot extrusion on the microstructure and anti-corrosion performance of LDHs conversion coating on AZ91D magnesium alloy. *Journal of Alloys and Compounds* 2019; 788: 756–767.
- [40] Pardo A, Merino MC, Coy AE, et al. Influence of microstructure and composition on the corrosion behaviour of Mg/Al alloys in chloride media. *Electrochimica Acta* 2008; 53: 7890–7902.
- [41] Esmaily M, Svensson JE, Fajardo S, et al. Fundamentals and advances in magnesium alloy corrosion. *Progress in Materials Science* 2017; 89: 92-193.
- [42] Aghion E, Perez Y. Effects of porosity on corrosion resistance of Mg alloy foam produced by powder metallurgy technology. *Materials Characterization* 2014; 96: 78–83.
- [43] Zhang SD, Wu J, Qi WB, et al. Effect of porosity defects on the long-term corrosion behaviour of Fe-based amorphous alloy coated mild steel. *Corrosion Science* 2016; 110: 57-70.